JCAMECH

Effect of Stress-Fiber Inclusion on the Local Stiffness of Cell Cytoskeleton Probed by AFM Indentation: Insights from a Discrete Network Model

Naeem Zolfaghari[a], Mahdi Moghimi Zand[a, b, *], Roozbeh Dargazany[b]

[a] Small Medical Devices, BioMEMS & LoC Lab, Department of Mechanical Engineering, University of Tehran, Tehran, Iran
[b] Department of Civel & Environmental Engineering, College of Engineering, Michigan State University

ARTICLE INFO

ABSTRACT

In this paper, we analyze the effect of stress-fiber inclusion on the stiffness of an actin random network. We use a discrete random network model to analyze the elastic response of this system in terms of apparent Young's modulus. First, we showed that for a flat-ended cylindrical indenter the total indentation force has a linear relation with the indentation depth and the indenter radius. Using this relation, we concluded that the stiffening effect of the stress-fiber on the fibrous network has a range of effectivity and surprisingly, the stiffening is not maximum when the stress-fiber is straight below the indenter but when it is a certain distance from it. These results shed light on some aspects of the widely used AFM stiffness measurements of cells.

1. Introduction

The cell cytoskeleton is a scaffold made up of biopolymer fibers, cross-linkers, and other proteins that grants Eukaryote cells their fascinating mechanical behavior [1]. Among these fibers, F-actin has the most prominent role in the stiffness of cells [2]. Using different cross-linkers, F-actin can create random networks, branched networks, and bundles [1]. A type of bundle that can be connected to the exterior of the cell is called actin stress-fiber [3] and is observed to have a direct relation with the cell stiffness variations in different stages of cancer development [4, 5].

The methods for the measurement of the stiffness of living cells can be divided into two main groups, namely, active and passive. Active methods apply an external force to the specimen and using its response to this force, the stiffness is calculated. On the other hand, passive methods do not use any external force. Atomic Force Microscopy (AFM) based methods can be classified as an active method [6]. Mainly, AFM consists of a cantilever beam with an attached tip with a specified geometry. For the measurement of the stiffness of a sample, the AFM tip is brought in contact with the top of the sample. As the tip is pushed down against the sample, the cantilever ends and knowing the stiffness of the beam, the applied force can be calculated. Then, using the deformation and the applied force, the stiffness can be calculated using appropriate formulas [7].

Using AFM, elasticity maps of living cells have been reported which contain stress-fibers within the loading region [8]. Results have shown that the stress-fibers have higher stiffness than the rest of the network as also observed in other experiments [9]. It is claimed that the stress-fiber under survey in this experiment is indented rather than bent. Also, it is observed that the stress-fibers cause an anisotropic deformation in AFM indentation experiments in that, using spherical indenter results in elliptical deformations with long axis along the stress-fibers [10]. The amount of actin stress-fibers is shown to be directly correlated to the stiffness in benign and malignant breast cancer cells using AFM experiments [4, 11]. Considering these experiments, here we use a computational approach to analyze the effect of stress-fiber inclusion on the stiffness of random actin networks when probed by AFM indentation. We are interested in knowing the relation between the depth of the stress-fibers with respect to the indentation surface and its effect on the enhancement of the local stiffness.

There are various approaches to model a random fibrous network such as the one in cell cytoskeleton [28]. Depending on the phenomena under study, continuum methods [12] or discrete random networks [13] can be chosen. The later has been successfully used to model local phenomena such as negative Poynting effect [14], bend-to-stretch phase transition [15, 16], and strain-stiffening [17] to name a few. The main merit of discrete network model over continuum models is that it is devoid of any homogenization assumptions that are the basis of the continuum approaches [18]. Consequently, we will use this method for our simulations.

Figure 1. Schematic of an AFM Measuring the Stiffness of Cell Cytoskeleton (Left: The Cell, Right: Simulation Box)

In the next section, we describe the modeling approach beginning with geometry creation and the simulation procedure for finite element modeling. Then, the results are proposed by first verifying the linear relation between the total indentation force and indentation depth on one hand, and AFM tip radius on the other. Finally, the addition of a stiff-fiber is studied.

2. Model Description

We are interested in the local stiffness of the cell cytoskeleton which contains an actin stress-fiber when measured using AFM indentation (Figure 1). In our simulations, we assume that this local stiffness is measured using AFM with a flat-ended cylindrical tip with a uniform cross-section throughout its length to avoid any complications due to the alterations in the contact area of the tip with the sample [19, 20]. Besides, it is shown that sharp tips will result in higher stiffness as they induce localized deformations [21]. It has been shown that for a flat-ended tip, the relation between the total force on the AFM tip and the indentation depth is linear, even for hyperelastic materials [22, 23]. We will recheck and verify this linearity in the results section for the random fibrous network. On the other hand, we will limit our simulations to indentation depths of 1% of the sample thickness to avoid stiffening due to the substrate which is below the limit of 5% due to Batra [24]. The effect of the aqueous medium, actin tread milling, cross-linker dynamics, and any possible motor activity is neglected for the sake of simplicity.

The geometry of the network is created on an FCC lattice crystal in 3D. The bonds of the lattice are chosen as the fibers of the network. Normally, an FCC lattice has a coordination number of 12. To reduce it, the bonds of the lattice are then removed with a probability p. This coordination number can be compared to the isostatic connectivity $z = 2d$ in d dimensions where a network of central forces is stable [25]. Central force means that the elements can only bear axial loads and no bending or torsional loads are tolerated by the fibers. The other limit is the bond percolation threshold below which there is no connected cluster spanning the box. This value for an FCC lattice is $p = 0.119$ [26]. An example of a network with $p = 0.3$ is shown in figure 2 with lattice constant 1 and box side length of 3.

The created geometry is then transformed into an input file for the finite element analysis using ABAQUS software. Each fiber is modeled using a 3D Timoshenko beam element (B31) [27]. In other words, each component of the network can bear axial,

lateral, and torsional loads. Linear elastic material properties and nonlinear geometry are assumed throughout the analysis. Two loading procedures are used; one for the evaluation of Young's modulus of the network and the other for the simulation of AFM indentation. For both loadings, the nodes on the opposite plane of the load are pinned and the four lateral planes are fixed in directions perpendicular to the direction of load. For the evaluation of Young's modulus, a displacement boundary condition is applied to the plane in the perpendicular direction while fixing the movements in the other two directions. For AFM indentation, circles with appropriate radius are chosen and the nodes within that circle are forced to move perpendicular to the
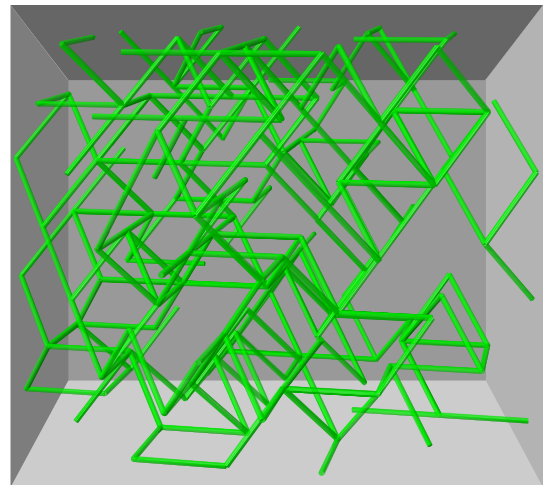

Figure 2. Simulation Box Using an FCC Lattice ($L_{Box} = 3$, $p = 0.3$)

plane of the circle while the movements in the two other directions of all the nodes on the top plane are fixed. This boundary condition is shown schematically in figure 3 for these two cases.

After finding the system equilibrium, the reaction forces of the nodes under loading and their displacements are collected. For the calculation of Young's modulus, the force is divided by the surface area of the box and the displacement is divided by the length of the box to obtain the stress-strain curves. Then, a line is fitted to this curve, the slope of which is reported as the apparent Young's modulus. For the AFM indentation case, the total force of the nodes (F_{Tot}) and the indentation depth (D_P) is used in the equation [22]
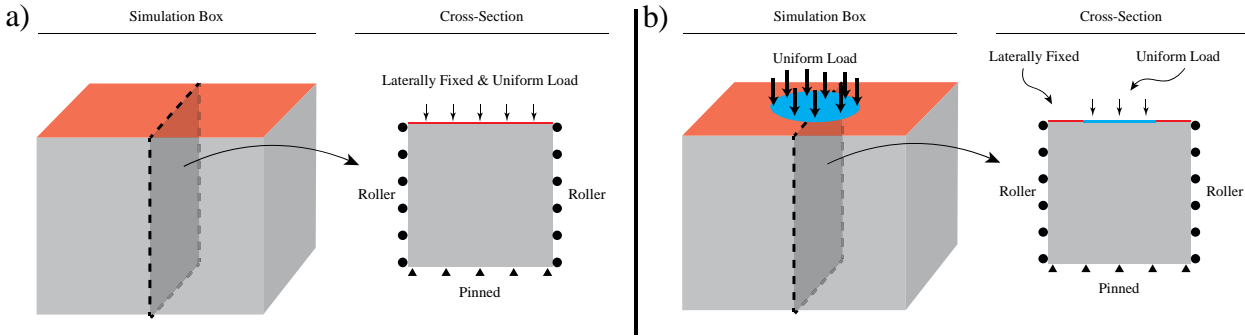
$$F_{Tot} = \alpha_0 E R_{AFM} D_P \qquad (1)$$

Figure 3. Boundary Conditions for the Calculation of Young's Modulus (a) and AFM indentation (b)

to extract the apparent Young's modulus E. R_{AFM} is the AFM tip radius and α_0 is a constant multiplication factor. In hyperelastic materials, the apparent Young's modulus depends on derivatives of the elastic energy with respect to the invariants of the deformation tensor [22]. The linear dependence of F_{Tot} on R_{AFM} and D_p needs be assured and will be checked in the next section.

3. Results and Discussions

Since we are dealing with a statistically created network (by stochastic dilution of bonds), the simulation box should be chosen large enough to have a statistically reliable sample. In addition, for small boxes, the boundary conditions will affect the results. Consequently, different networks with $p = 0.3$ ($z \approx 3.6$) are constructed and loaded axially. For each box size, 5 network realizations are simulated. The stress-strain curves were linear up to strains of 1.5% but for later results, strains of up to 1.0% are used for the calculation of Young's modulus. The nonlinearity for higher strains is due to the orientation of fibers which is of no concern in this paper. An example of the stress-strain curve of the simulation box is shown in figure 4. Therefore, a linear line was fitted to them and the slope of this line is used as the Young's modulus of the network. Since the quantitative value of Young's modulus of the fibers did not affect the linear response (up to a multiplication factor), all the results are reported after division by Young's modulus of the fibers.
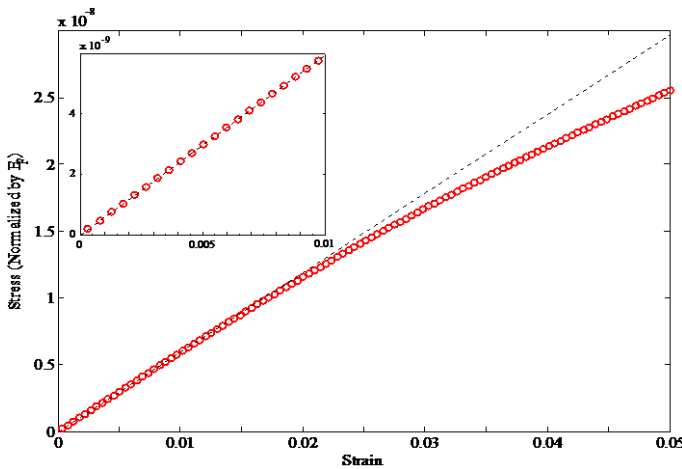

Figure 4. Stress-Strain curve of the Simulation Box ($L_{Box} = 10$, $p = 0.3$) (Circles: Results of Simulation, Dashed Line: Fitted Linear Curve); Inset: Enlarged Data Up to 1% Strain
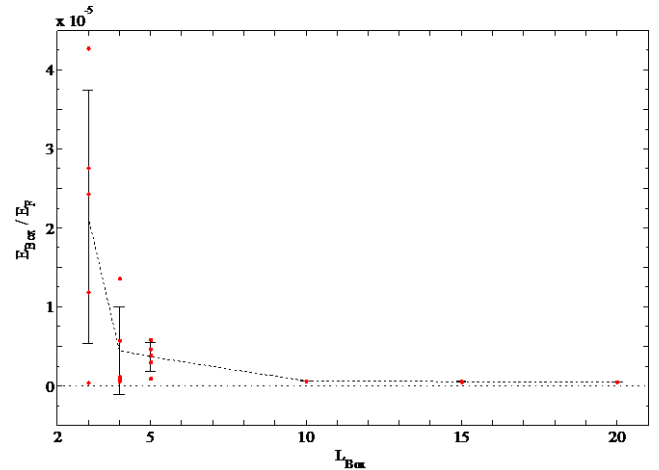

Figure 5. Normalized Young's Modulus of Network vs. Box Size ($p = 0.3$)

Figure 5 shows Young's modulus of networks with different box sizes. The dots show the result of individual simulations and the dotted line and the error bars show their average and standard deviation, respectively. As is obvious, networks with small box size predict higher Young's moduli for the network as the boundary conditions constrain a large part of the network and therefore, increase the stiffness of the network unrealistically. In addition, the results of small boxes show a large deviation due to statistical under-sampling. As the size of the simulation box increases, the stiffness converges as these two effects diminish. Considering this, the box size of 10 is chosen for the later simulations. Next, the nodes on the top plane of the network which lie inside a circle of radius R_{AFM} are loaded, as explained in the last section. This is similar to an indentation using a flat-ended cylindrical AFM tip. The total reaction force of these nodes is depicted against their displacement in figure 6.a for box size 10 and $R_{AFM} = 1.5$ as an example. Circles show the data of simulation and the lines are the linear fits. As can be seen, there is a linear relation between the indentation depth and the total force. The slope of these curves are depicted against the radius of loading circle in figure 6.b. The trend of the average value of tests is shown as a dashed line and the fitted line is shown as a solid green line. The linear relation between R_{AFM} and the dF_{Tot}/dD_p can also be observed here. It is noted that when the size of load circles becomes comparable to the size of the simulation box ($R_{AFM} = 5$), the data show a deviation from the linear response. In summary, figure 6.b verifies the validity of equation 1 for discrete networks. Using the values of Young's moduli evaluated in figure 4, the multiplication factor α_0 is calculated as 1.93 ± 0.08.
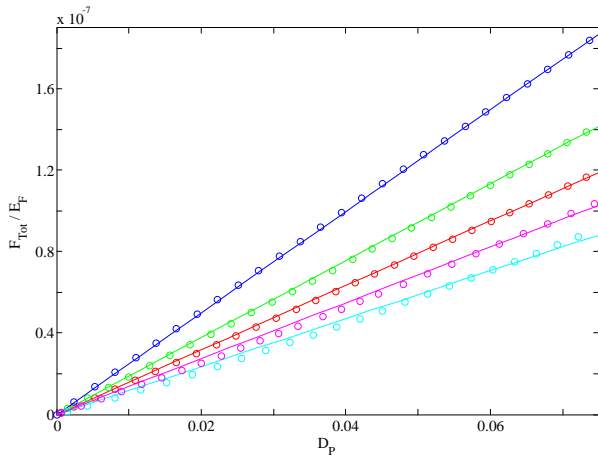
a) Total Force vs. Indentation Depth ($R_{AFM} = 1.5$)
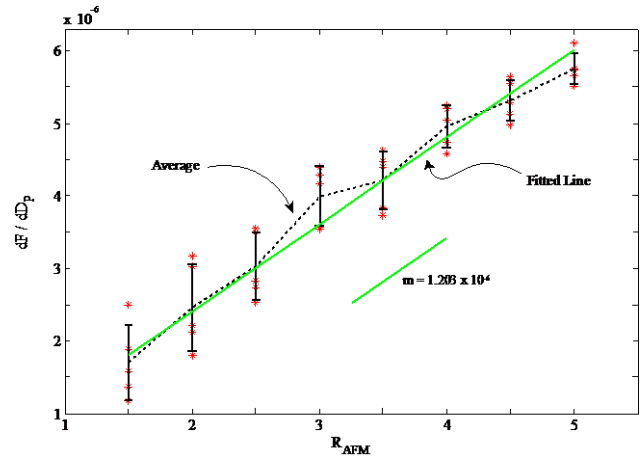
b) dF_{Tot} / D_P vs. R_{AFM}

Figure 6. Relative Local Stiffness of Network vs. AFM Tip Radius ($L_{Box} = 10$, $p = 0.3$)

Now that the details of the evaluation of the apparent Young's modulus using AFM simulation have been grounded, we will study the effect of inclusion of a stress-fiber within the network. To do this task, we place a stress-fiber in the middle of the box at different depths with respect to the top plane of the box where the AFM indentation is imposed. The circle of the AFM has a radius of 2 and the box and its density are the same as before, i.e. $L_{Box} = 10$, $p = 0.3$. To get rid of the multiplication factor α_0 and the AFM tip radius of equation 1, all of the results are reported as the ratio of the slope of F_{Tot} versus D_P lines for networks with a stress-fiber and the same network without one. This ratio will represent the relative apparent Young's moduli in the two networks which can then be used to study the effect of stress-fibers on the local stiffness of the network. The relative Young's modulus is depicted in figure 7 versus the stress-fiber depth. Moving the stress-fiber from the top of the box to the bottom, the measured Young's modulus decreases to the value of a network without a stress-fiber with the maximum value of the Young's modulus occurring when the stress-fiber is located at 0.5 below the surface. Therefore, the addition of a stress-fiber increases Young's modulus of the network in general but the increase is localized and depends on the distance between the load and the stress-fiber axis.

three cases of stress-fiber depth: at the top and 0.5 and 3 units below the surface. When the stress-fiber is located at the top of the network and straight under AFM load, the maximum stress will be more localized than the other cases. On the other hand, sinking the stress-fiber to 0.5 units below the surface helps distribute the stress better and therefore, the stiffening effect of the stress-fiber will work better. This is the cause of the maximum value in the relative Young's modulus of figure 7. The deeper the stress-fiber is located, the smaller the magnitude of the tolerated stress by it will be. Therefore, smaller amounts of stress can be distributed by the stress-fiber. The consequence of this is that the farther the distance between the stress-fiber and the load becomes, the lesser the stiffening resulting from the addition of the stress fiber. It seems that the effective region of the stress distribution is a circle of radius 2 (i.e. the radius of the loading circle). Consequently, when the stress-fiber is located at a depth of 3 units or below, the increase in Young's modulus of the network with a stress-fiber compared to a network without one becomes less than 3%. In other words, the stress will be totally carried by the network and the effect of the stress-fiber will be insignificant. In this way, for small indentations, the range of effectiveness of the stress-fibers is comparable to the radius of the loading circle.

It is noted that in some situations, the measured Young's modulus is smaller than the overall Young's modulus since there are statistical fluctuations in the network stiffness, the average of which results in the overall Young's modulus. This is the reason that the average value of the relative stiffness is below 1 when the stress-fiber is located at the bottom of the box.

4. Conclusions

In this research, a discrete random fibrous network is used to study the effect of stress-fibers on the stiffness of the actin network. We first showed that the initial response of the network without a stress-fiber is linear under uniform compression. The stress-strain curves up to 1% strain were used to evaluate the Young's modulus of the network. We then simulated the AFM indentation in the network and showed that the total indentation force has a linear relation with the indentation depth and the indenter radius when the indenter is a flat-ended cylinder. Using this fact, we analyzed the response of the network when a stress-fiber is included in the network. Results showed that this inclusion increases the stiffness of the network but the stiffening effect is localized. The larger the distance between the stress-fiber axis and the indentation surface, the smaller the stiffening will be. In addition, we showed that the stiffening is not maximum when the stress-fiber is located at the top surface but when it is a little below it.
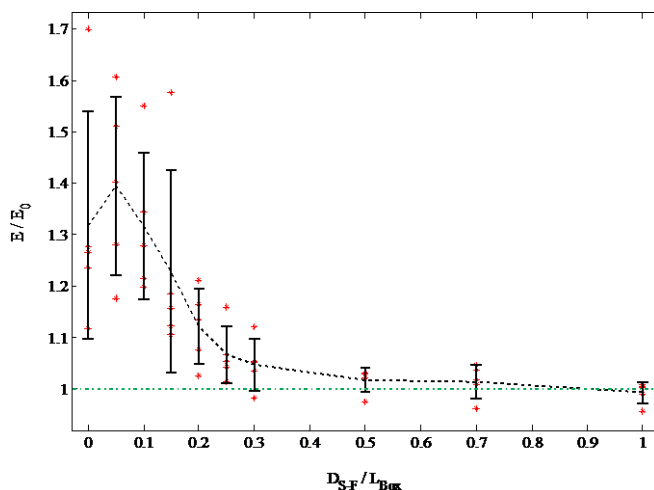

Figure 7. Young's Modulus of Network with a Stress-Fiber (E) Relative to the Same Network without a Stress-Fiber (E_0) vs. Stress-Fiber Depth($p = 0.3$, $L_{Box} = 10$)

To better analyze the mechanism of this increase, the stress distribution in the fibers of the network is shown in figure 8 for

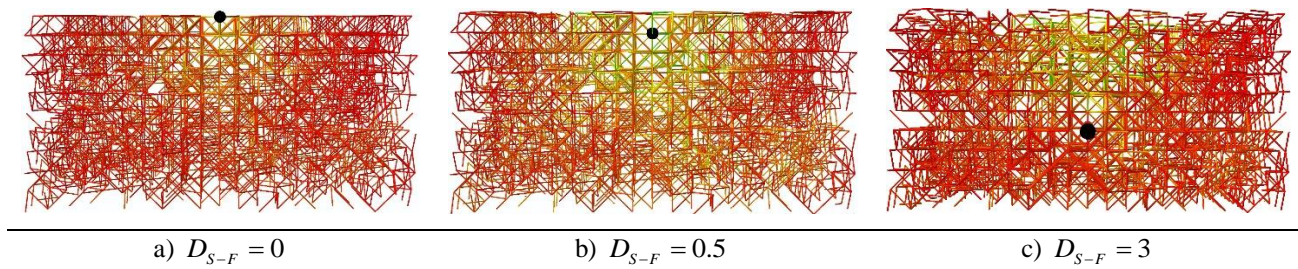a) $D_{S-F} = 0$ b) $D_{S-F} = 0.5$ c) $D_{S-F} = 3$

Figure 8. Localization of the Stress for Networks with a Shallow Stiff-Fiber (Maximum Stress: Green, Minimum Stress: Red, Stress Fiber: Black Circle)

References

[1] B. Alberts, A. Johnson, J. Lewis, M. Raff, K. Roberts, P. Walter, Molecular biology of the cell. Garland science, *New York*, pp. 1227-1242, 2007.

[2] H. Haga, S. Sasaki, K. Kawabata, E. Ito, T. Ushiki, T. Sambongi, Elasticity mapping of living fibroblasts by AFM and immunofluorescence observation of the cytoskeleton, *Ultramicroscopy,* Vol. 82, No. 1-4, pp. 253-258, 2000.

[3] S. Tojkander, G. Gateva, P. Lappalainen, Actin stress fibers–assembly, dynamics and biological roles, *J Cell Sci,* Vol. 125, No. 8, pp. 1855-1864, 2012.

[4] A. Calzado-Martín, M. Encinar, J. Tamayo, M. Calleja, A. San Paulo, Effect of actin organization on the stiffness of living breast cancer cells revealed by peak-force modulation atomic force microscopy, *ACS nano,* Vol. 10, No. 3, pp. 3365-3374, 2016.

[5] N. Wang, M. Zhang, Y. Chang, N. Niu, Y. Guan, M. Ye, C. Li, J. Tang, Directly observing alterations of morphology and mechanical properties of living cancer cells with atomic force microscopy, *Talanta,* Vol. 191, pp. 461-468, 2019.

[6] M. R. Mofrad, Rheology of the cytoskeleton, *Annual Review of Fluid Mechanics,* Vol. 41, pp. 433-453, 2009.

[7] A. Alessandrini, P. Facci, AFM: a versatile tool in biophysics, *Measurement science and technology,* Vol. 16, No. 6, pp. R65, 2005.

[8] L. Lu, S. J. Oswald, H. Ngu, F. C.-P. Yin, Mechanical properties of actin stress fibers in living cells, *Biophysical journal,* Vol. 95, No. 12, pp. 6060-6071, 2008.

[9] K. D. Costa, A. J. Sim, F. C. Yin, Non-Hertzian approach to analyzing mechanical properties of endothelial cells probed by atomic force microscopy, *Journal of biomechanical engineering,* Vol. 128, No. 2, pp. 176-184, 2006.

[10] Y. M. Efremov, M. Velay-Lizancos, C. J. Weaver, A. I. Athamneh, P. D. Zavattieri, D. M. Suter, A. Raman, Anisotropy vs isotropy in living cell indentation with AFM, *Scientific reports,* Vol. 9, No. 1, pp. 5757, 2019.

[11] Q. Li, G. Y. Lee, C. N. Ong, C. T. Lim, AFM indentation study of breast cancer cells, *Biochemical and biophysical research communications,* Vol. 374, No. 4, pp. 609-613, 2008.

[12] M. J. Unterberger, K. M. Schmoller, A. R. Bausch, G. A. Holzapfel, A new approach to model cross-linked actin networks: multi-scale continuum formulation and computational analysis, *Journal of the mechanical behavior of biomedical materials,* Vol. 22, pp. 95-114, 2013.

[13] C. P. Broedersz, X. Mao, T. C. Lubensky, F. C. MacKintosh, Criticality and isostaticity in fibre networks, *Nature Physics,* Vol. 7, No. 12, pp. 983, 2011.

[14] E. Conti, F. C. MacKintosh, Cross-linked networks of stiff filaments exhibit negative normal stress, *Physical review letters,* Vol. 102, No. 8, pp. 088102, 2009.

[15] C. Broedersz, M. Sheinman, F. MacKintosh, Filament-length-controlled elasticity in 3D fiber networks, *Physical review letters,* Vol. 108, No. 7, pp. 078102, 2012.

[16] S. B. Lindström, A. Kulachenko, L. M. Jawerth, D. A. Vader, Finite-strain, finite-size mechanics of rigidly cross-linked biopolymer networks, *Soft Matter,* Vol. 9, No. 30, pp. 7302-7313, 2013.

[17] G. Žagar, P. R. Onck, E. van der Giessen, Two fundamental mechanisms govern the stiffening of cross-linked networks, *Biophysical journal,* Vol. 108, No. 6, pp. 1470-1479, 2015.

[18] M. J. Unterberger, G. A. Holzapfel, Advances in the mechanical modeling of filamentous actin and its cross-linked networks on multiple scales, *Biomechanics and modeling in mechanobiology,* Vol. 13, No. 6, pp. 1155-1174, 2014.

[19] K. Costa, F. Yin, Analysis of indentation: implications for measuring mechanical properties with atomic force microscopy, *Journal of biomechanical engineering,* Vol. 121, No. 5, pp. 462-471, 1999.

[20] E. K. Dimitriadis, F. Horkay, J. Maresca, B. Kachar, R. S. Chadwick, Determination of elastic moduli of thin layers of soft material using the atomic force microscope, *Biophysical journal,* Vol. 82, No. 5, pp. 2798-2810, 2002.

[21] R. Vargas-Pinto, H. Gong, A. Vahabikashi, M. Johnson, The effect of the endothelial cell cortex on atomic force microscopy measurements, *Biophysical journal,* Vol. 105, No. 2, pp. 300-309, 2013.

[22] J. Humphrey, H. R. Halperin, F. C. Yin, Small indentation superimposed on a finite equibiaxial stretch. Implications for cardiac mechanics, *Journal of Applied Mechanics, Transactions ASME,* Vol. 58, No. 4, pp. 1108-1111, 1991.

[23] M. Beatty, S. Usmani, On the indentation of a highly elastic half-space, *The Quarterly Journal of Mechanics and Applied Mathematics,* Vol. 28, No. 1, pp. 47-62, 1975.

[24] R. Batra, Quasistatic indentation of a rubberlike layer by a rigid cylinder, in *Proceeding of,* 345-357.

[25] J. C. Maxwell, L. on the calculation of the equilibrium and stiffness of frames, *The London, Edinburgh, and Dublin Philosophical Magazine and Journal of Science,* Vol. 27, No. 182, pp. 294-299, 1864.

[26] D. Stauffer, A. Aharony, 2018, *Introduction to percolation theory*, Taylor & Francis,

[27]   V. Abaqus, 6.14 Documentation, *Dassault Systemes Simulia Corporation,* Vol. 651, 2014.

[28]   N. Zolfaghari, M. Moghimi Zand, and R. Dargazany. "Local Response of Actin Networks is Controlled by Tensile Strains in The Stress-Fibers: Insights from a Discrete Network Model." International Journal of Applied Mechanics, In press.